

Up-Scaled Petrophysical Analyses Using Micro-Level Field-Of-View Petrographic Images for the Kapuni Group, Taranaki Basin, New Zealand*

Aamer Alhakeem¹, Kelly Liu¹, and Waleed H. Al-Bazzaz²

Search and Discovery Article #10953 (2017)**

Posted June 19, 2017

*Adapted from extended abstract based on poster presentation given at AAPG 2017 Annual Convention and Exhibition, Houston, Texas, United States, April 2-5, 2017

¹Affiliation1 Geology and Geophysics, Missouri S&T, Rolla, MO United States (alhakeem.a@gmail.com)

²Kuwait Institute for Scientific Research, Ahmadi, Kuwait

Abstract

This paper presents the results of pore level microanalyses and characterization of the Kapuni Group sandstone reservoir in the Taranaki Basin, New Zealand. In Well Maui-7, three rock fragments of the Mangahewa Formation, situated at depths of 2736 m, 2796 m, and 2897 m, are selected for analyses. In addition, two rock fragments of the Kaimiro Formation, situated at depths of 3011 m and 3028 m, are analyzed. After sample preparation, various petrographic images are captured with a thin section microscope at different depths of magnification. The images are then processed to study the pore networks in the space domain between a lower bound of 50 μm and an upper bound of 4 mm. Then, petrophysical parameters such as porosity, permeability, and MHR are measured at their native selected spaces (Al-Bazzaz and Al-Mehanna, 2007). The well logs, including density, neutron, resistivity, GR, and SP, are analyzed to calculate the porosity and permeability logs. Neural network processing is conducted by combining the morphological pore sample and well log analyses for the training of the computer. Using the consistent data measured and delineated from different field-of-view (FOV), up-scaling porosity, matrix permeability, MHR, and grain-size at micro-levels are investigated effectively. The petrophysical parameters obtained from up-scaling FOV scale sizes are utilized to develop a simple statistical model. The sample size scale to be measured includes 600X-FOV, which is adequate for recognizing features at 50 μm -scale size, then gradually escalates to 450X-FOV for recognizing features at 100 μm -scale size, 300X-FOV for features at 200 μm -scale size, 100X-FOV for features at 500 μm -scale size, and finally, 40X-FOV for features at 2 mm-scale size.

Introduction

The Taranaki Basin, a Cretaceous foreland basin, covers an area of about 330,000 km² mostly in the offshore along the west coast of the North Island, New Zealand (King et al., 2010). Due to its great potential and wide promising, various data including geological, geophysical, and petrophysical data are collected and processed to predict reservoir characteristics using relative fast, inexpensive, and reliable methods. The “Big data” analyses produce QC petrophysical log analysis, logs modification, and up scaling. Three approaches, i.e., morphological approach, well log analyses, and computational neural networking modeling, are utilized to investigate data from micro- to meter-level.

Objectives

Three rock fragments from the Mangahewa Formation are analyzed in this study. The objectives include:

- To qualify and quantify the pores and the nature of the pore network in the formation
- To describe the wettability of the formation
- To study the porosity and the relative permeability action of internal influences of pore and grain morphology
- To measure porosity, relative permeability, and Mean Hydraulic Radius (MHR) (pore-throat)
- To invest in the “Big data” available from the basin to extract valuable hidden information and patterns for fast, inexpensive, and reliable reservoir characterization
- To provide QC tool for the petrophysical log analysis using lower scale level thin sections which provide significant amount of petrophysical measurements

Data and Method

The data were provided by the Ministry of Business, Innovation, and Employment (MBIE) in New Zealand. The dataset includes 2D/3D seismic surveys, composite well data, geological data (core lab data, thin sections, etc.), geophysical data, drilling data, production data, and reports, which can be processed as “Big data” to extract hidden valuable information and patterns. In Well Maui-7, three rock fragments of the Mangahewa Formation, situated at depths of 2736 m, 2796 m, and 2897 m, are selected for analyses ([Figure 1](#)). In addition, two rock fragments of the Kaimiro Formation, situated at depths of 3011 m and 3028 m, are analyzed. After sample preparation, various petrographic images are captured with a thin section microscope at different depths of magnification.

Petrophysical analyses by morphological approach are implemented using the thin section images of Maui-7 ([Figure 2](#)) to conduct a study if the pore networks in the space domain between a lower bound of 50 μm and an upper bound of 4 mm ([Table 1](#)). The thin sections are scanned and analyzed using the visual analysis tool, which counts different pores and grains based on pre-identified classes of pore sizes ranges ([Table 1](#)) beside measuring their shapes, sizes, and distribution ([Table 2](#) and [Table 3](#)). Petrophysical parameters such as porosity, permeability, and MHR are measured at their native selected spaces according to the method proposed by Al-Bazzaz and Al-Mehanna (2007) ([Table 4](#)). Wettability, as described in [Table 1](#), is predicted for each sample and is classified as shown in [Figure 3](#).

Petrophysical well log analyses are conducted by using density, neutron, resistivity, GR, and SP logs to calculate the porosity and permeability logs (Asquith and Krygowski, 2004). The morphological analysis of the thin sections provides spatial measurements along the wellbore. However, with such big data available for the formation, petrophysical parameters can be computed along the formation by correlating with measured petrophysical core data and log. The Well Maui-7 data are utilized to associate a precise up scaling of the micrometer domain thin section data to meter domain logs. Computational approaches of analyses are conducted by combining the morphological pore sample, core data, and well log analyses for the Neural Network Training (NNT) ([Figure 4](#)). Then, Neural Network Model (NNM) is performed for further predictions. The porosity log of Well Maui-5 was predicted with more realistic results as shown in [Figure 4](#) in the NNM input and output.

Using the consistent data measured and delineated from different field-of-view (FOV), up-scaling porosity, matrix permeability, MHR, and grain-size at micro-levels are investigated effectively.

Result and Discussion

The morphological analyses of the thin section (TS) practically match the results of core lab and well log analysis. The challenges in calculating the porosity from the morphological approach is the black stain in the thin section images that affect the porosity measurements. However, with better geological and petrophysical background involved with such big data, accurate decisions made to describe such features.

Sample TS1 at 2736 m has three unique pore distributions, extremely tight, moderately tight and large pores. At the beginning, 3,443 pores are captured, selected, and counted from 2X thin section image. All pores are grouped in 10 classes for pre-logic measurements, and these 10 classes are generated from the 3,443 claimed big data. Subsequently each class was subject to post logic calculations ([Table 3](#)), which yielded 10 interesting pore morphology and petrophysical attributions summarized in [Table 4](#). Out of all distribution, three zones are subject for discussion. Zone A (extremely tight) is defined by classes 1, 2 and 3. It has the most available pores abundance 29%, 2.4%, and 1.1% and an equivalent pore diameter of 2.0, 4.8, and 6.2 μm respectively. The porosity is low in class 1, which is about 6%, but high in classes 2 and 3, which are 24.1%, 34.7% respectively. The permeability is calculated to be 55 md, 166 md, and 232.5 md respectively. The pore-throat (MHR) is approximated to be 3.1 μm , 5.1 μm , and 5.7 μm respectively. The wettability is approximated to be 179, 169, and 150 indicating that zone A is strongly-oil-wet. Zone A is then described as low in oil production and it will need EOR recovery enhancement. Zone B has 4 classes (4, 5, 6, and 7). They are bigger in area than zone A but less in abundance than zone A, roughly around 1% in total. The equivalent diameters are 7.4 μm , 8.3 μm , 9.1 μm , and 9.9 μm . The porosity for zone B is doubled roughly about 50%, which is better than zone A, and the average permeability is about 350 md. The wettability is described as a transition from strongly-oil-wet (171° and 174°) in classes 3 and 5 respectively to medium-oil-wet (119° and 125°) in classes 6 and 7 respectively. Zone B will show an increase in water production later in the formation development cycle. This zone is a candidate for water flooding secondary recovery. Zone C is classes 8, 9, and 10 and shows the greatest pore area, but the least abundance, about 0.2% in total. However, their pore equivalent diameters are the greatest, 11.0 μm , 11.4 μm and 12.1 μm . Zone C pore style and size will be responsible for the easy flow regime within the formation. In respect with zone A and zone B, zone C shows the greatest porosity regime, >50% and the greatest permeability regime, over than 400 md. The average pore throat for zone C is 10.3 μm . The wettability is described between moderately-oil-wet to moderately-water-wet, indicating that zone C is the main primary oil recovery region in the formation. Zones A, B, and C are unique and have different characterization signatures; however, the overall average behavior of the TS1 sample including all three zones yields a pore diameter equivalent of 1.3 μm , average porosity of 21.6%, average permeability of 47.5 md, a pore throat connecting diameter of 7.8 μm , and contact angle wettability of 113 creating an overall medium-oil-wet reservoir conditions. Water flooding is highly recommended for 2736 m depth.

For samples TS2, 2796 m and TS3 2897 m ([Table 3](#)), and the same analyses as sample TS1 were conducted. TS2 has about 1494 count of pores. TS3 has about 17,339 counts of pores. Both samples have 3 zones of pore networks zone A, zone B, and zone C. Sample TS2 has zones A and B strongly-oil-wet, but zone C has strong-water-wet to medium-oil-wet indicating better oil recovery than sample TS1 ([Table 4](#)). TS2 has an average porosity of 16.1%, an average permeability of 783 md, and an average pore-throat (MHR) of 4.1 μm . The overall wettability contact

angle is 109 medium-oil-wet. Sample TS3 has also three distinctive production zones. Zone A is described as strongly-oil-wet, zone B as medium-oil-wet, and zone C as strongly-water-wet regimes. The average porosity is 16.9 % and the average permeability is 332 md. The average pore-throat (MHR) is 4.4 μm , which is better than sample TS2. The sample TS3 will show fast oil recovery due the combination effect of highest number of pores, water wet wettability, high permeability and MHR.

The integration of the porosity well log analysis of Maui-7 as input porosity curve with the thin section analysis and the core lab data using the neural network training yielded more realistic and confident porosity log ([Figure 4](#)) for the NNT output curve. The NNM was built based on the training of the logs with the TS and core lab data. The NNM predicted an enhanced porosity curve of Well Maui-5 by minimizing the fluctuating in the beginning of the log as shown in [Figure 4](#) for the NNM predicted curve.

Conclusions

1. Three zones were successfully measured, A (the smallest), B (the middle), and C (the largest). Zone A is described to be strongly-oil-wet, zone B is described to be medium-oil-wet, and zone C is either medium-oil-wet or strongly-water-wet depending on the size area of the pore. The larger the pore, the more likely follow water wet regimes.
2. The more abundance of pores, the more likely increase in permeability. The higher area of pores just as zone C in the formation, the higher potential of oil recovery.
3. Porosity and permeability average values can be different than core data, for the imaging processing can capture all classes of pore networks (zones A, B, and C); while core analyses cannot accurately penetrate to zone A type of networks.
4. Zone A oil recovery is a candidate for EOR, zone B for water flooding secondary recovery and zone C for primary recovery, all regimes are available in different proportions in the same formation.
5. TS1 has the lowest oil recovery potential. TS2 has better oil recovery system than TS1. TS3 has the greatest oil recovery potential.
6. Porosity of (16.5 – 21.6%), permeability of (47.5 – 782.5 mD), and MHR of (4.1 – 7.8 μm) with medium to strong oil wet wettability indicate that the Mangahewa Formation is a good reservoir, which is consistent with the previous studies.
7. The neural network model offered a valuable tool for pseudo well log predictions for this area.

Acknowledgments

We express our sincere gratitude to the New Zealand Government for providing the data and to the Saudi Ministry of Higher Education for sponsoring Mr. Aamer Alhakeem. Thanks to Mr. Haidar Almubarak, PhD candidate in Computer Engineering at Missouri S&T, for his computational support.

References Cited

Al-Bazzaz, W.H., and Y.W. Al-Mehanna, 2007, Porosity, Permeability, and MHR calculations using SEM and thin-section images for complex Maaddud-Burgan carbonate reservoir characterization: Society of Petroleum Engineers, SPE 110730.

Asquith, G., and D. Krygowski, 2004, Basic well log analysis, second edition: American Association of Petroleum Geologists and Society of Exploration Geophysicists, Methods in Exploration.

Tiab, D. and E.C. Donaldson, 2004, Petrophysics, second edition: Gulf Professional Publishing.

Higgs, K.E., M.J. Arnot, G.H. Browne, and E.M. Kennedy, 2010, Reservoir potential of Late Cretaceous terrestrial to shallow marine sandstones, Taranaki Basin, New Zealand: Marine and petroleum geology, v. 27/9, p. 1849-1871.

King, P.R., G.P. Thrasher, K.J. Bland, P. Carthew, D. D'Cruz, A.G. Griffin, C. M. Jones, and D.P. Strogon, 2010, Cretaceous-Cenozoic geology and petroleum systems of the Taranaki Basin, New Zealand. Digitally remastered version: GNS Science, Lower Hutt, Institute of Geological & Nuclear Sciences monograph.

New Zealand Petroleum and Minerals (NZPAM), 2014, New Zealand Petroleum Basins: New Zealand Ministry of Business, Innovation and Employment, Wellington, New Zealand, ISSN 2324-3988.




Sample Info	Thin Section Image
<p data-bbox="716 183 865 215">Sample# 1</p> <p data-bbox="703 269 877 383">Formation: Mangahewa C-Sand</p> <p data-bbox="737 440 844 513">Depth: 2736 m</p>	<p data-bbox="919 151 1283 183">2xpl View Width 4000 μm</p> 
<p data-bbox="716 596 865 628">Sample# 2</p> <p data-bbox="703 682 877 795">Formation: Mangahewa C-Sand</p> <p data-bbox="737 852 844 925">Depth: 2796 m</p>	<p data-bbox="919 563 1283 596">2xpl View Width 4000 μm</p> 
<p data-bbox="716 1008 865 1040">Sample# 3</p> <p data-bbox="703 1094 877 1208">Formation: Mangahewa C-Sand</p> <p data-bbox="737 1265 844 1338">Depth: 2897 m</p>	<p data-bbox="919 976 1283 1008">2xpl View Width 4000 μm</p> 

Figure 1. Three thin section sample images and their information from Well Maui-7.

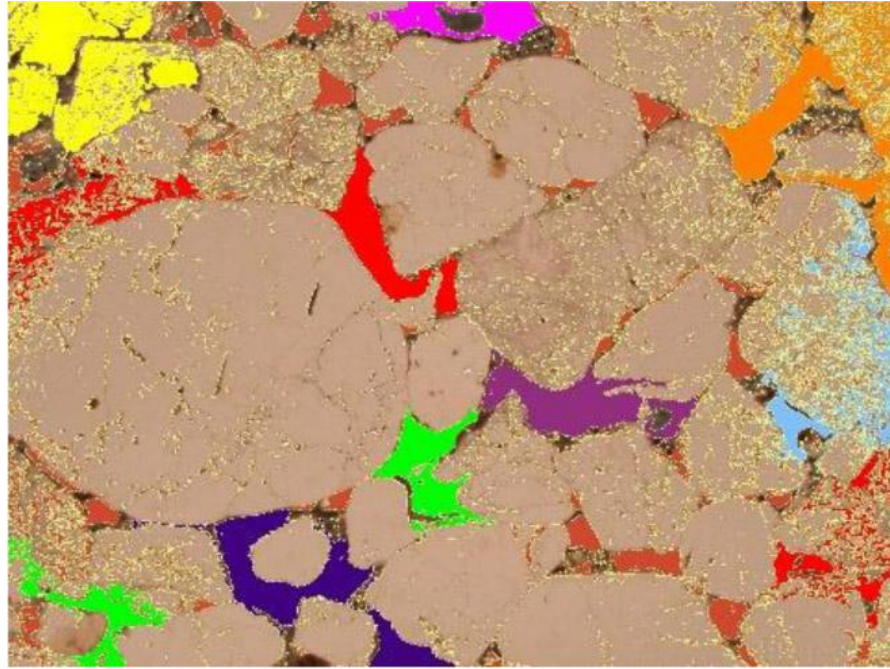


Figure 2. Thin section sample# 3 from Maui-7 showing the classes identification of the pore area ranges.

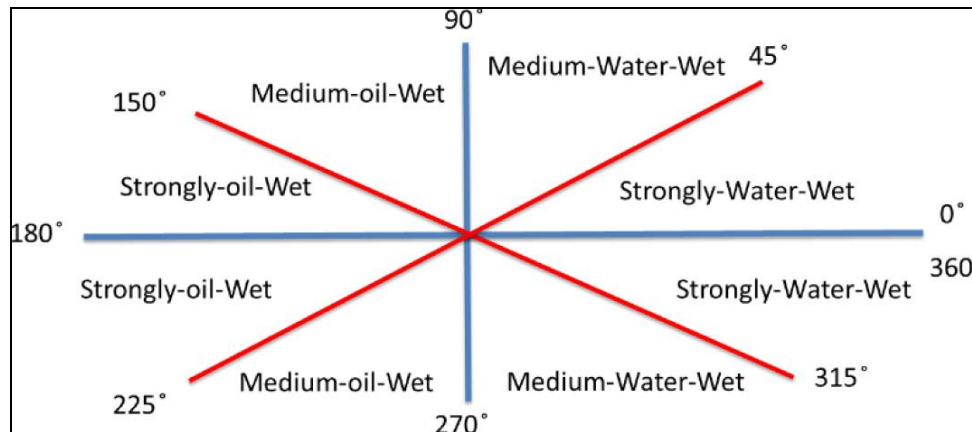


Figure 3. Classification of pore wettability (Al-Bazzaz, 2017).

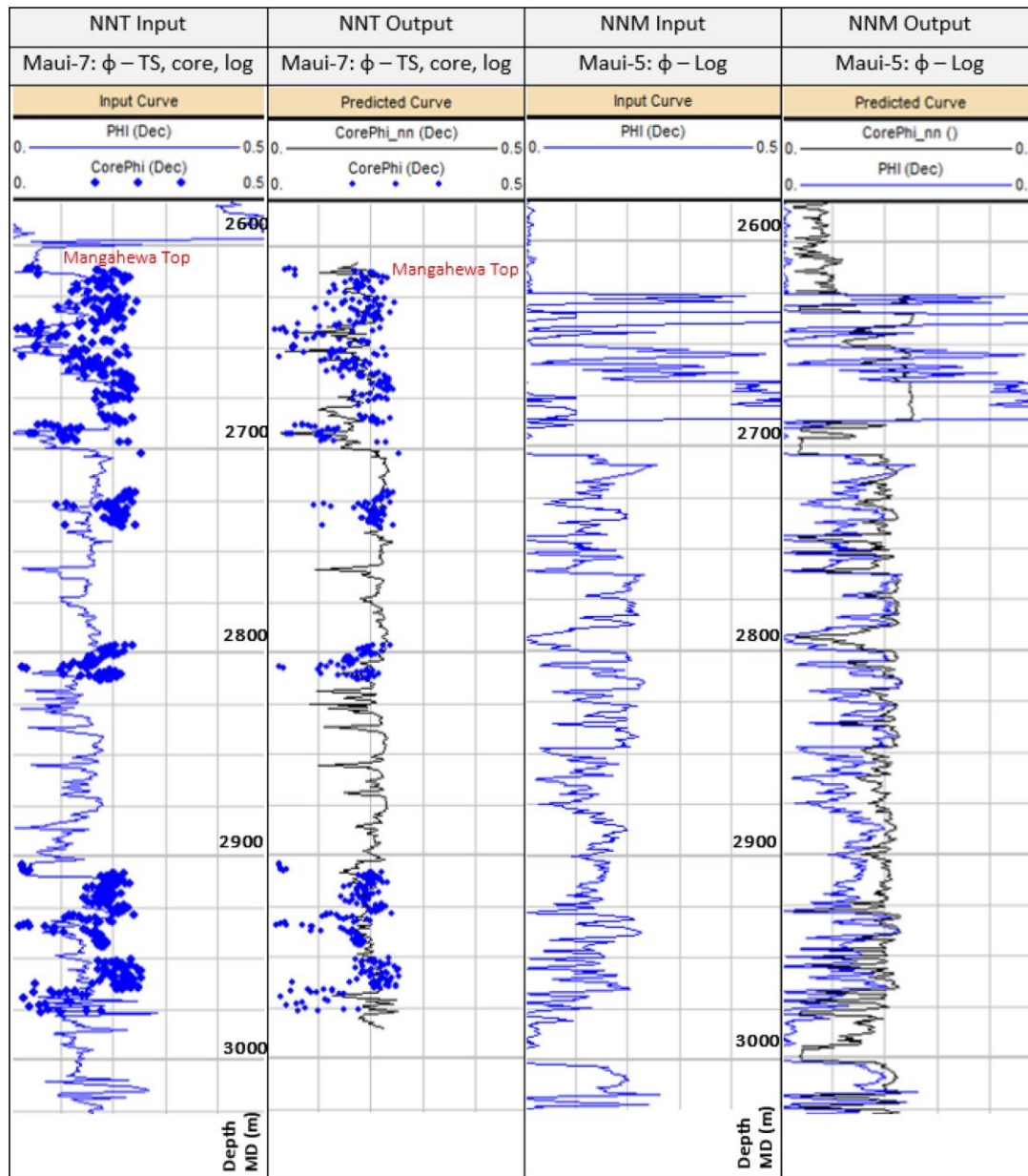


Figure 4. The first two columns shown the neural network training input and output for Maui-7 that include the porosity (ϕ) log from well analysis (Phi log) and the thin section results with core lab porosity data. The two last columns shown neural network modeling input (blue) and output (black).

Parameter	Method	Units	Approach	Description	Comments
Pore Area	Σ Pore Area	$\mu\text{-m}^2$	Visual Counting	Measured	Accurate
Grain Area	Σ Grain Area	$\mu\text{-m}^2$	Visual Counting	Measured	Accurate
Pore Perimeter	Pore Circumference	$\mu\text{-m}$	Visual Counting	Measured	Accurate
Porosity	$\phi = \frac{\sum PoreArea}{\sum PoreArea + \sum GrainArea}$	Fraction	Summation / Statistical	Calculated	Low Error
Hydraulic Radius	$HydraulicRadius = \frac{PoreArea}{PorePerimeter}$	$\mu\text{-m}$	By Definition	Calculated	Avoid Circular or Triangular Shape Simplicity
Mean Hydraulic Radius (MHR)	$MHR = \frac{\sum_1^n HydraulicRadius}{n}$	$\mu\text{-m}$	Averaging/ Statistical	Calculated	Pore Throat for a Sample
The Long L-axis of a Grain Particle	L-axis	$\mu\text{-m}$	Visual Counting	Measured	Accurate
The Short L-axis of a Grain Particle	S-axis	$\mu\text{-m}$	Visual Counting	Measured	Accurate
The Intermediate I-axis of a Grain Particle	$I = \frac{L + S}{2}$	$\mu\text{-m}$	Mid-point Averaging	Calculated	Simple Approach
Grain Diameter	$GrainDiameter = \frac{I}{1.32}$	$\mu\text{-m}$	Kumar & Cui Sieve Method	Calculated	Originally Applied for mm-scale Grain Particles
Permeability	$k = 5.6281 \cdot \frac{d^2 \cdot \phi^3}{(1 - \phi)^2}$	Milli-Darcy	Carmen & Kozeny	Calculated	Diameter & Porosity are Accurately Measured
Class Pore Area	Total Pore Areas Fitted in a Range of Pore Areas where MHR is Located	$\mu\text{-m}^2$	Visual Counting	Measured	Accurate
Wettability	Θ = Pore Shapes and Morphology	Degrees	Pore/grain Orientations (New Proposal)	Measured	2-D

Table 1. Definitions of the morphological analysis parameters (Al-Bazzaz and Al-Mehanna, 2007).

Class (1-10)	Area Range [μm^2]
1	1-500
2	500-1000
3	1000-1500
4	1500-2000
5	2000-2500
6	2500-3000
7	3500-4000
8	4000-4500
9	4500-5000
10	5000-10000
Total	1-10000

Table 2. Identification of ten classes for the pore area size ranges applied to each thin section sample from ([Figure 1](#)).

Morphological Pore Analysis (Pre-Logic) Mean Values											
Class	Frequency [%]	Area [μm^2]	Perimeter [μm]	Elongation	Roundness	Circularity	Width [μm]	Length [μm]	W/L	Equivalent	Angle [$^\circ$]
1	29.10	28.5	9.1	1.9	2.5	1.3	1.8	3.4	2.0	2.0	179.0
2	2.35	140.8	28.4	3.7	2.6	0.7	4.6	8.6	2.0	4.8	169.4
3	1.05	235.0	41.5	4.8	2.3	0.5	6.3	11.2	1.9	6.2	150.1
4	0.55	333.5	48.5	4.6	2.2	0.5	7.7	12.9	1.7	7.4	171.0
5	0.26	424.4	53.7	4.3	3.0	0.7	7.5	16.2	2.2	8.3	174.2
6	0.09	512.7	63.9	5.0	2.8	0.5	9.4	17.7	1.9	9.1	119.0
7	0.09	594.7	75.6	6.3	2.5	0.4	10.1	18.1	1.9	9.9	125.0
8	0.03	741.7	71.4	4.3	2.7	0.6	10.0	20.7	2.1	11.0	17.0
9	0.12	801.6	86.9	6.4	2.0	0.3	11.6	19.1	1.6	11.4	117.8
10	0.06	903.3	66.8	3.1	2.0	0.6	11.7	19.8	1.7	12.1	179.0
TS1 Total	100.0	21.4	5.4	1.5	3.1	2.1	2	1.1	0.5	1.3	113.0
1	14.06	78.1	45.5	2.3	2.4	1.0	8.5	15.4	0.6	9.4	179.0
2	2.07	338.5	120.7	3.6	2.5	0.7	19.5	35.0	0.6	20.7	144.0
3	1.27	566.1	166.5	4.1	2.2	0.6	28.4	45.6	0.6	26.8	169.0
4	0.80	818.6	201.9	4.2	2.6	0.6	31.8	59.8	0.5	32.3	156.7
5	0.47	1031.7	261.0	5.4	2.5	0.5	39.0	65.2	0.6	36.2	174.5
6	0.33	1243.2	295.2	5.9	2.1	0.4	45.6	76.5	0.6	39.8	158.2
7	0.27	1409.8	240.8	3.3	2.6	0.8	39.2	73.6	0.5	42.4	143.6
8	0.27	1676.3	411.7	8.8	2.3	0.3	51.5	84.1	0.6	46.2	52.0
9	0.07	1947.4	408.2	6.8	3.9	0.6	47.8	108.3	0.4	49.8	73.3
10	0.07	2148.8	364.4	4.9	2.8	0.6	55.4	109.1	0.5	52.3	105.5
TS2 Total	100.0	78.6	24.9	1.5	2.4	1.6	4.6	8.0	0.6	4.9	109.0
1	9.395	26.0	29.9	2.72	3.8	1.4	4.3	8.3	0.5	4.21	179.3
2	0.006	3033.6	508.5	5.10	6.8	1.3	42.7	170.7	0.3	62.20	178.1
3	0.012	3992.0	1133.3	1.86	28.8	15.5	105.6	142.6	0.7	71.28	142.1
4	0.017	5641.8	1691.1	2.59	43.7	16.9	98.6	186.7	0.5	84.74	132.9
5	0.006	6525.8	995.6	4.09	12.1	3.0	76.6	190.6	0.4	91.22	6.9
6	0.006	8191.1	1684.5	3.44	27.5	8.0	110.0	316.2	0.3	102.20	29.1
7	0.006	10460.8	4907.8	1.95	183.0	94.0	136.8	249.2	0.5	115.50	81.7
8	N/A	N/A	N/A	N/A	N/A	N/A	N/A	N/A	N/A	N/A	N/A
9	0.006	12931.8	1654.8	0.58	16.8	28.8	139.1	173.4	0.8	128.41	5.9
10	0.006	15194.0	3150.6	0.99	51.9	52.4	199.6	285.2	0.7	139.19	78.0
TS3 Total	100.0	7.6	5.2	2.3	1.3	0.6	1.0	1.7	0.6	1.10	72.3

Table 3. Pre-Logic morphological pore mean values calculations of the thin section samples from [Figure 1](#) using the parameter definitions in [Table 1](#) and the classes of area ranges from [Table 2](#).

Post-Logic				
Class	Wettability	ϕ [%]	K [mD]	MHR [μm]
1	strongly-oil-wet	6.05	54.91	3.14
2	strongly-oil-wet	24.14	166.14	4.96
3	medium-oil-wet	34.68	232.51	5.66
4	strongly-oil-wet	42.97	284.84	6.88
5	strongly-oil-wet	48.95	322.58	7.90
6	medium-oil-wet	53.67	352.38	8.03
7	medium-oil-wet	57.33	375.55	7.87
8	strongly-water-wet	62.63	409.01	10.39
9	medium-oil-wet	64.43	420.37	9.23
10	strongly-oil-wet	67.12	437.36	13.53
TS1 Total	medium-oil-wet	21.60	47.53	7.80
1	strongly-oil-wet	16.40	778.82	1.72
2	Medium-oil-wet	45.95	2011.04	2.81
3	strongly-oil-wet	58.71	2544.83	3.40
4	strongly-oil-wet	67.27	2903.43	4.05
5	strongly-oil-wet	72.15	3107.50	3.95
6	strongly-oil-wet	75.74	3257.73	4.21
7	medium-oil-wet	77.98	3351.35	5.86
8	strongly-water-wet	80.80	3469.78	4.07
9	medium-water-wet	83.02	3562.65	4.77
10	medium-oil-wet	84.37	3618.87	5.90
TS2 Total	medium-oil-wet	16.48	782.52	4.10
1	strongly-oil-wet	0.01	0.00	0.87
2	strongly-oil-wet	0.78	1.11	5.97
3	medium-oil-wet	1.03	2.55	3.52
4	medium-oil-wet	1.45	7.27	3.34
5	strongly-water-wet	1.68	11.30	6.55
6	strongly-water-wet	2.10	22.54	4.86
7	medium-water-wet	2.69	47.51	2.13
8	N/A	0.00	0.00	0.00
9	strongly-water-wet	3.32	90.93	7.81
10	medium-water-wet	3.90	149.28	4.82
TS3 Total	medium-water-wet	16.95	332.49	4.43

Table 4. Post-Logic morphological pore mean value calculations of the thin section samples from Figure 1 using the parameter definitions in Table 1 and the classes of area ranges in Table 2. The Post-Logic calculations include the Wettability, Porosity (ϕ), Permeability (K), and pore-throat (MHR).